


Structuring Hydrogel Surfaces for Tribology

Journal Article**Author(s):**

Gombert, Yvonne; Simič, Rok; Roncoroni, Fabrice; [Dübner, Matthias](#) ; Geue, Thomas; Spencer, Nicholas D.

Publication date:

2019-11-22

Permanent link:

<https://doi.org/10.3929/ethz-b-000381782>

Rights / license:

[Creative Commons Attribution-NonCommercial 4.0 International](#)

Originally published in:

Advanced Materials Interfaces 6(22), <https://doi.org/10.1002/admi.201901320>

Funding acknowledgement:

669562 - Polymer Analogs to Biolubrication Systems: Novel materials for exploring cartilage tribology and exploiting its mechanisms (EC)

Structuring Hydrogel Surfaces for Tribology

Yvonne Gombert, Rok Simič, Fabrice Roncoroni, Matthias Dübner, Thomas Geue, and Nicholas D. Spencer*

Hydrogels are often used as model systems for articular cartilage due to similarities in their tribological properties. However, neither the structures nor the friction mechanisms of either system are fully understood. A key aspect of hydrogel lubrication is the nature of the polymeric structure at the surface, and the lubricating water film. A combination of neutron reflectometry and infrared spectroscopy is used to probe polymer volume fraction from the interface into the bulk hydrogel and its dependence on the molding material. The depth dependence of the polymer-network density influences the compressibility of the hydrogel surfaces, as demonstrated by both atomic force microscopy (AFM)- and micro indentation. By changing molding materials, substantial differences in the gradient of polymer-network density are observed with depth. The lower the volume fraction of polymer at the hydrogel surface, the more water it can maintain at its interface as a substantial water film that is stable even under static conditions. Such films render the hydrogel highly lubricious, with a speed-independent friction coefficient of $\mu = 0.01$, measured in gemini contact. This result provides experimental evidence that the presence of these highly lubricious water films is strongly dependent on the polymer-network structure at the surface.

the opinion that, unlike fluid-film lubrication in engineered joints, the tribology of cartilage is dominated by a combination of boundary lubrication and the load support of pressurized, interstitial cartilage fluid.^[2] With this combination, cartilage achieves friction coefficients of less than $\mu = 10^{-3}$, even at high system pressures.

The materials showing the greatest potential to emulate the friction coefficient of this natural tribological system are hydrogels. These are chemically cross-linked, macromolecular, hydrophilic polymers, with their interstitial space filled with large amounts of water. Since they were proposed by Wichterle and Lim^[3] in the 1960s as polymers that can be used in permanent contact with living tissue, their application has been steadily increasing, especially in the biomedical sector.^[4] Their outstanding combination of properties—mechanical stability, excellent conformability, remarkable diffusion properties,

oxygen permeability, transparency, and biocompatibility—makes this class of soft synthetic materials ideal for biomedical use.

Whenever hydrogels come into contact with human tissue, the interaction between the gel surface and the tissue plays a decisive role in the successful application of the material in the body. Therefore, it comes as no surprise that the tribology of hydrogels—in parallel to research into cartilage tribology—is an active topic of investigation among scientists in the soft-matter-tribology community. Several theories on hydrogel tribology have emerged from different studies that all aim to explain the cartilage-like coefficient of friction and to better understand this synthetic lubrication system. Despite many structural similarities between cartilage and hydrogel and their comparably low coefficients of friction, it is the subject of an ongoing debate as to how closely related the tribological principles of cartilage and hydrogels actually are.^[5]


The classic work of Gong et al. led to the repulsion-adsorption model for the friction of hydrogels.^[6,7] The model focuses on the interactions taking place at the interface between sliding partners, the friction being determined by the attractive and repulsive tendencies between the polymer chains at the hydrogel surface and the sliding partner. In the repulsive case, a liquid film forms between the shearing bodies, which promotes lubrication and lowers friction. In the adsorptive case, friction is increased by the elastic deformation of polymer chains adsorbed on the counter surface. Factors influencing the adsorption can be mesh size and charge density of the polymeric network or salt concentration in the solvent.

1. Introduction

The frictional properties of articular cartilage have fascinated scientists for centuries.^[1] Cartilage being a water-based system, its lubrication mechanisms contrast dramatically with those of man-made, oil-lubricated machine joints. Our understanding of how nature maintains low friction and wear of mammalian joints for the lifetime of the organism has become increasingly sophisticated over the last 30 years. The scientific community is increasingly of

Y. Gombert, Dr. R. Simič, F. Roncoroni, Dr. M. Dübner, Prof. N. D. Spencer
Laboratory for Surface Science and Technology
Department of Materials
ETH Zürich
Vladimir-Prelog-Weg 5, 8093 Zürich, Switzerland
E-mail: nspencer@ethz.ch

Dr. T. Geue
Laboratory for Neutron Scattering
Paul Scherrer Institute (PSI)
Forschungsstrasse 111, 5232 Villigen, Switzerland

 The ORCID identification number(s) for the author(s) of this article can be found under <https://doi.org/10.1002/admi.201901320>.

© 2019 The Authors. Published by WILEY-VCH Verlag GmbH & Co. KGaA, Weinheim. This is an open access article under the terms of the Creative Commons Attribution-NonCommercial License, which permits use, distribution and reproduction in any medium, provided the original work is properly cited and is not used for commercial purposes.

The copyright line for this article was changed on 25 October 2019 after original online publication.

DOI: 10.1002/admi.201901320

Another approach from Pitenis and Sawyer aims to define hydrogel friction as a material property, in order to disconnect it from the classically accepted understanding of friction as a system property.^[8] With the help of scaling concepts from polymer physics, they demonstrate the theoretical dependence of system properties such as contact area, contact pressure, and shear stress, as well as the elastic modulus, and permeability of the hydrogel, on the mesh size of the gel. This approach allows for the prediction of hydrogel friction based solely on a knowledge of the hydrogel mesh size. Backed up with experimental evidence, they conclude that the higher the proportion of liquid phase in the gel, the better the hydrogels can lubricate.

Although the two theories differ fundamentally in their approach, one parameter that plays a dominating role in both theories is the polymer volume fraction at the hydrogel surface. This quantity is not simply determined by the total mass ratio of polymer to liquid phase in the hydrogel, since the polymer volume fraction can vary greatly with the sample depth and depends sensitively on the substrate used in the manufacturing process. Gong et al. have extensively studied the substrate effect for many hydrophilic vinyl monomer hydrogels produced by free radical polymerization.^[7,9,10] According to their work, chemically identical hydrogels with the same volume fraction of polymer can have different polymer structures at the surface and thus lead to different frictional responses. Therefore, precise knowledge of the change in polymer and solvent volume fractions from the surface down to the bulk hydrogel is essential for a detailed understanding and targeted design of hydrogel friction.

In this work, we explore the progression of polymer volume fraction from the hydrogel surface into its bulk in a detailed fashion. On two opposing hydrogel surface structures we reveal, experimentally, how the polymer volume fraction affects the liquid film at the hydrogel interface, how the elasticity of the material changes with sample depth, and how these properties influence the frictional behavior. Using a combination of spectroscopic and mechanical analysis techniques, we are able to follow the relationship between polymer volume fraction and mechanical and frictional properties from the single nanometer range up to 100 μm into the hydrogel sample. We demonstrate, first, that the substrate has neither a direct chemical influence nor a roughness influence on the hydrogel surface during free radical polymerization. Second, we show the presence of a substantial liquid film at the interface of hydrogels with low surface polymer volume fraction that enables speed-independent lubrication over a wide velocity range. We believe that this further evolution in our knowledge of hydrogel surface

structure will both facilitate a more detailed understanding of hydrogel tribology and enable the establishment of design criteria for lubricious hydrogels.

2. Results and Discussion

2.1. Substrate Properties before and after Polymerization

A crucial step in the examination of the substrate effect on hydrogel surface properties is to consider a potential chemical interaction between the mold and the initial and emerging components of the free-radical polymerization of the polyacrylamide (pAAM) hydrogel. For this purpose, the roughness and the hydrophilicity of glass and polydimethylsiloxane (PDMS) molds were measured before and after the hydrogel polymerization, as described in Section 2. The roughness of piranha-cleaned glass slides changed by 0.3 to a final root mean square roughness, R_q , of 1.0 nm after 24 h in contact with the radical reaction mixture (Table 1). The advancing and receding contact angles of the glass substrate showed complete wetting and no change in hydrophilicity after hydrogel polymerization. The ethanol-rinsed PDMS surfaces revealed a similarly smooth surface as the glass slides. Here, the R_q changed by 0.7 to 5.4 nm (within the measurement precision). While the advancing water contact angle of PDMS did not change during hydrogel polymerization, the contact angle hysteresis increased by 5°. This small change of contact angle hysteresis was in accordance with the minor roughness increase.

With a surface roughness below 6 nm on both mold surfaces, we consider them to be comparably smooth for the purposes of this work. This also allows us to exclude the influence of residual oxygen, trapped at the surface of rough molds, on hydrogel polymerization as was discussed in other studies.^[10] On both substrate materials, we find only marginal changes in roughness and contact angle. Therefore, we can rule out the influence of a strong chemical interaction between the substrate and the components in the radical polymerizing solution of pAAM as a cause for the hydrogel substrate effect.

2.2. Polymer Volume Fraction at the pAAM Hydrogel Surface

We used two characterization techniques, namely neutron reflectometry (NR) and infrared spectroscopy (Attenuated total reflectance Fourier-transform infrared, ATR-FTIR), to determine

Table 1. The R_q roughness and dynamic contact angles (advancing, θ_{adv} , and receding, θ_{rec}) of the glass and PDMS substrate materials were measured. Neither the roughness nor the contact angles reveal significant alterations of the substrates due to the free-radical polymerization of pAAM hydrogel.

		R_q ^{a)} [nm]	θ_{adv} ^{b)}	θ_{rec} ^{c)}
Hydrophilic glass	Before polymerization	0.7 (0.1)	Complete Wetting	Complete wetting
	After polymerization	1.0 (0.6)	Complete wetting	Complete wetting
Hydrophobic PDMS	Before polymerization	4.7 (0.5)	119° (3°)	82° (1°)
	After polymerization	5.4 (0.7)	117° (2°)	75° (3°)

^{a)} R_q : Root mean square roughness; ^{b)} θ_{adv} : Advancing contact angle; ^{c)} θ_{rec} : Receding contact angle.

the polymer volume fraction in the pAAm hydrogel surface. For this purpose, the samples were compressed to different degrees during a measurement. In this way, we effectively extended the measurement range of the devices, gaining information about the polymer distribution and compressibility of the hydrogels several micrometers into the samples.

2.2.1. Neutron Reflectometry

NR is a high-resolution analysis technique for interfaces and surfaces. We exploit it to analyze how the polymer density alters over the first 500 Å into the hydrogel surface.

Figure 1a,b shows the NR raw data in the low-wave-vector region for hydrophilic- and hydrophobic-molded hydrogels in comparison to pure D₂O. (Reflectivity spectra of the entire wave-vector range can be found in the Supporting Information.) Even from the raw data, we observed a decrease in neutron reflectivity with sample compression, which was more pronounced for the hydrophilic glass-molded hydrogel than it was for the hydrophobic PDMS-molded hydrogel. A drop in neutron reflectivity corresponds to a rise in the polymer volume

fraction within the detectable sample volume. Depth-resolved information on the change in neutron scattering-length density (SLD) from the silicon–hydrogel interface into the sample was achieved by fitting the raw data as described in detail above (Figure 1c,d). For the hydrophilic glass-molded hydrogel, we detected a drop in SLD compared to the pure D₂O line—even before compression was applied to the system. This reduction in SLD occurred gradually from the interface down into the hydrogel. It translates as a direct contact of the hydrogel polymer with the Si surface of the measurement device and an increase in polymer volume fraction with increasing distance from the surface. Upon compression of the hydrogel, both effects were amplified. Thus, we have uniform sample compression with volume preservation in the bulk and for the hydrogel surface. Figure 1c displays this distinct increase in polymer density accompanied by a decrease of D₂O from the interface down to 500 Å from the hydrogel surface. No pure water layer was detected between the Si surface and the hydrophilic glass-molded hydrogel.

In contrast, the SLD of the hydrophobic PDMS-molded hydrogel did not decrease within the first 100 Å from the Si block (Figure 1d). Instead, a thin layer of water separated the hydrogel

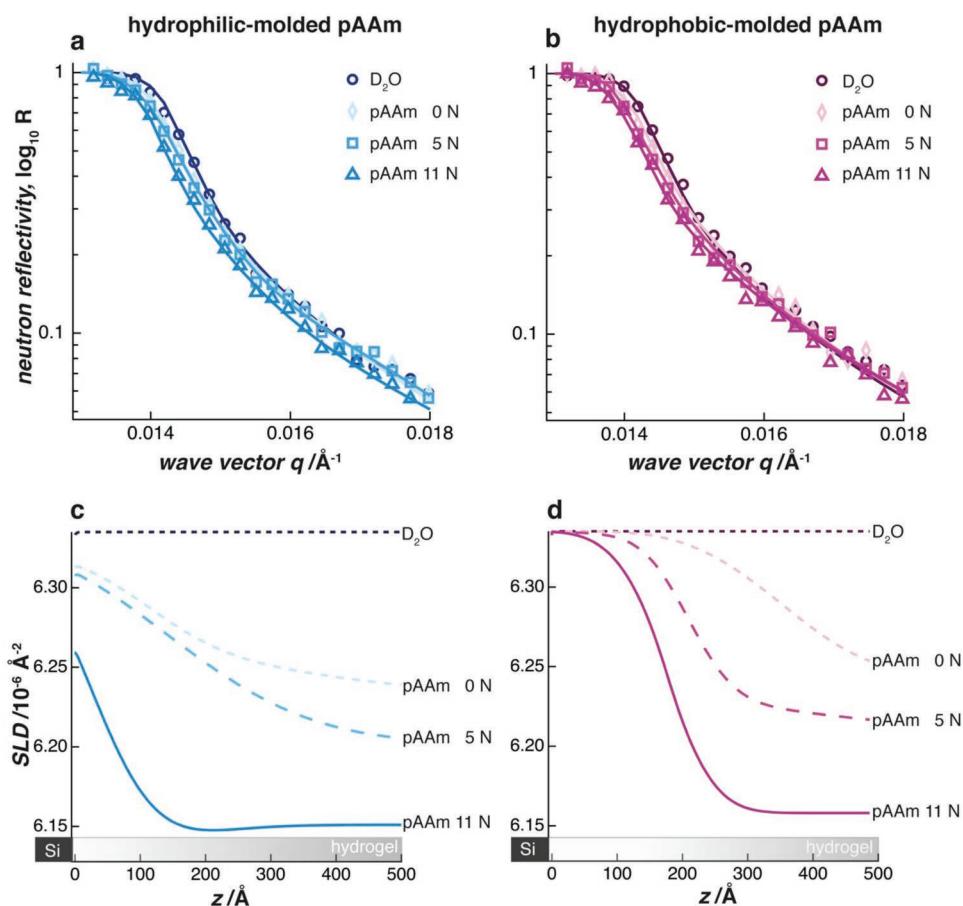


Figure 1. NR spectra of chemically equivalent hydrophilic glass-molded a,c) and hydrophobic PDMS-molded b,d) pAAm hydrogels display the influence of the amount of polymer at the interface on the neutron reflectivity. The raw data in panels (a) and (b) show the change in neutron reflectivity with normal force applied to push the hydrogels down onto the silicon block. The spectra in panels (c) and (d) illustrate the resulting scattering-length-density progression from the silicon block surface ($z = 0$) into the hydrogel. The gray bars on the z -axis indicate the position of the silicon block and the hydrogel surface relative to the plotted data.

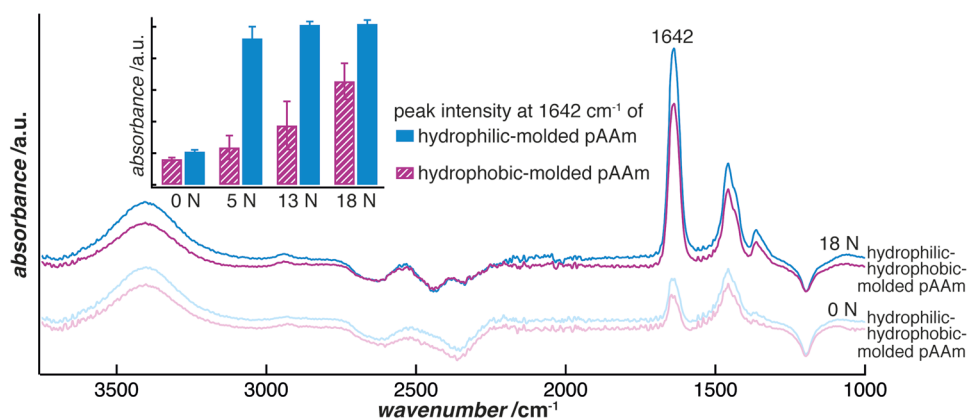


Figure 2. ATR-FTIR spectra of glass-molded (■) pAAm hydrogel reveal considerably stronger peaks characteristic of the polymer than the chemically equivalent PDMS-molded (□) pAAm hydrogel under load. The spectra are shifted vertically for clarity. The bar chart shows the carbonyl peak (1642 cm^{-1}) intensity evolution with normal force applied to push the hydrogel down onto the IR crystal.

polymer from the Si block. Only after 100 \AA did the SLD drop, revealing the presence of an increasing amount of polymer with sample depth. Our measurements provide evidence that this interfacial water film between the Si block and the hydrophobic-molded hydrogel is stable. Even though its thickness reduced upon compression, it never disappeared from the sample interface. Therefore, it continuously prevented a direct contact between the hydrogel polymer network and the Si block of the measurement device. However, the trend of increasing polymer density with sample compression, as observed for the hydrophilic-molded hydrogel, was also observed for the hydrophobic-molded samples beyond the stable water film at the surface. From this, we can infer that the volume within the hydrogel surface region is not conserved under compression and the compression is nonuniform, while the bulk of the hydrogel remains volume-conserving under uniform compression.

For hydrophilic glass-molded hydrogels, our measurements reveal a distinct increase in polymer volume fraction coupled with a decrease of water amount from 0 down to 500 \AA into the hydrogel surface. This contrasts with measurements on the hydrophobic PDMS-molded hydrogels, which show an increase in polymer volume only behind a continuous and permanent water film. This water film remained stable under all compressions applied in this work.

2.2.2. Infrared Spectroscopy

ATR-FTIR measurements were conducted with the same setup and on the same sample set as the NR measurements. With its shallow detection range and high resolution, the NR measurements focused on the polymer distribution at the interface between the hydrogel and its immediate surroundings. ATR-FTIR has a detection range of $1\text{--}2\text{ }\mu\text{m}$. The compression of the samples allowed us to extend this range to probe changes in polymer density for several micrometers from the hydrogel surface into the sample.

ATR-FTIR spectra of both hydrophilic glass- and hydrophobic PDMS-molded hydrogels showed the same peaks over the entire wavenumber range (Figure 2). This demonstrates that

the samples, whose chemical structures are dominated by an excess amount of monomer over cross-linker, were chemically identical and shows that the difference between them had a purely structural origin. (A detailed peak interpretation can be found in the Supporting Information.)

We followed the polymer distribution in the hydrogel surface with sample compression by IR absorbance analysis of the carbonyl peak at 1642 cm^{-1} (Figure 2, bar chart). At zero compression, spectra of both hydrophilic- and hydrophobic-molded hydrogels were characterized by similarly low peak intensities. Upon compression, the carbonyl peak of the hydrophilic-molded sample jumped to high relative absorbance. More polymer was detected in direct contact with the ATR-FTIR crystal. This high relative peak intensity and thus the high polymer volume fraction in the hydrogel increased only slightly with compression. It follows that the surface-near region of this hydrogel is comprised of a structure with a largely homogeneous polymer distribution with little compressibility. By contrast, the carbonyl peak of the hydrophobic-molded hydrogel rose step-wise with every loading-force increase. Thus, the sample surface region collapsed further, and more polymer was detected upon increasing compression. Nevertheless, its relative absorbance always remained significantly lower than that of the hydrophilic-molded hydrogel. Thus, our data reveal an entirely different polymer distribution for the hydrophobic-molded hydrogels. Here, the step-wise rise in ATR-FTIR absorbance of the carbonyl group with applied load suggests a pronounced densification and decrease in compressibility of the hydrogel polymer with increasing distance into the sample. That the volume is not conserved at this hydrogel surface upon compression is in line with our findings from NR experiments of the nonuniform nature of the compression.

In addition to the variation in carbonyl peak intensity, all sample spectra indicated a decrease of D_2O signal with compression at peak positions 2628 and 2442 cm^{-1} . This reduction in ATR-FTIR absorbance, which again was more pronounced for the hydrophilic-molded hydrogel, indicates a squeezing out of the water upon sample compression.

In summary, our findings of an even polymer distribution in the near-surface regions of hydrophilic-molded hydrogels and a polymer gradient with strongly reduced total polymer volume

on hydrophobic-molded hydrogels correlate well with the results of NR evaluation. They also extend the trends observed at the hydrogel interface up to several micrometers into the bulk hydrogel.

2.3. Elastic Modulus of pAAm Hydrogel

In order to investigate the mechanical properties of a hydrogel surface as a function of its molding conditions, we performed indentation measurements from the low micrometer range to 100 μm into the sample. Subsequently, we were able to correlate the depth-dependent elastic modulus of the sample with our findings from the spectroscopic analysis.

2.3.1. Atomic Force Microscopy Nanoindentation

The force response to indentation of the topmost surface layer of pAAm hydrogels was measured by means of atomic force microscopy (AFM) nanoindentation. Information about the change in elastic modulus from the sample interface down into the hydrogel surface was obtained by fitting the raw data with the Hertz model.

The hydrophilic glass-molded hydrogel showed a sharp force onset upon indentation (Figure 3a). Here, the Hertzian fit matched the experimental data perfectly and revealed an elastic modulus of 11 kPa that already plateaued at 600 nm indentation depth (Figure 3b). In contrast, the hydrophobic PDMS-molded hydrogel demonstrated a low force onset upon indentation. While the hydrophilic-molded hydrogel showed a force response of 10 nN at an indentation depth of 0.4 μm , the hydrophobic-molded hydrogel reached the same force level only at the tenfold deeper indentation of 4 μm . Thus, the surface elastic modulus of this sample remained well below that of the hydrophilic-molded hydrogel. This considerably lower force response could not be accurately modeled with a Hertzian fit, which showed an overestimation of the indentation force in the uppermost layer of the hydrophobic-molded hydrogel.

Overall, for the hydrophilic-molded hydrogel surface, the significant force increase starting from contact, as well as the stable elastic modulus, reveals a largely uniform hydrogel polymer distribution with little compressibility. Such behavior is usually associated with regular cross-linking of the polymer network. Only if the polymer network is evenly cross-linked up to the surface, is it able to directly counteract externally applied compression with such instantaneous and strong force response. Conversely, the weak force onset and the small slope in elastic modulus on the hydrophobic-molded hydrogel surface imply a greatly diminished overall polymer density that seems to increase gradually with surface depth. This low resistance to compression is reminiscent of the compression behavior of polymer brushes. In polymer brushes, chains are not chemically cross-linked. Here, a compression only causes the deformation of individual chains in the contact surface, resulting in a low overall force response. Therefore, our measurements allow us to draw the conclusion that the mesh size decreases with increasing polymer volume fraction as a function of sample depth. The varying precision of the Hertzian fit additionally indicates a substantial difference between these two hydrogel surface types.

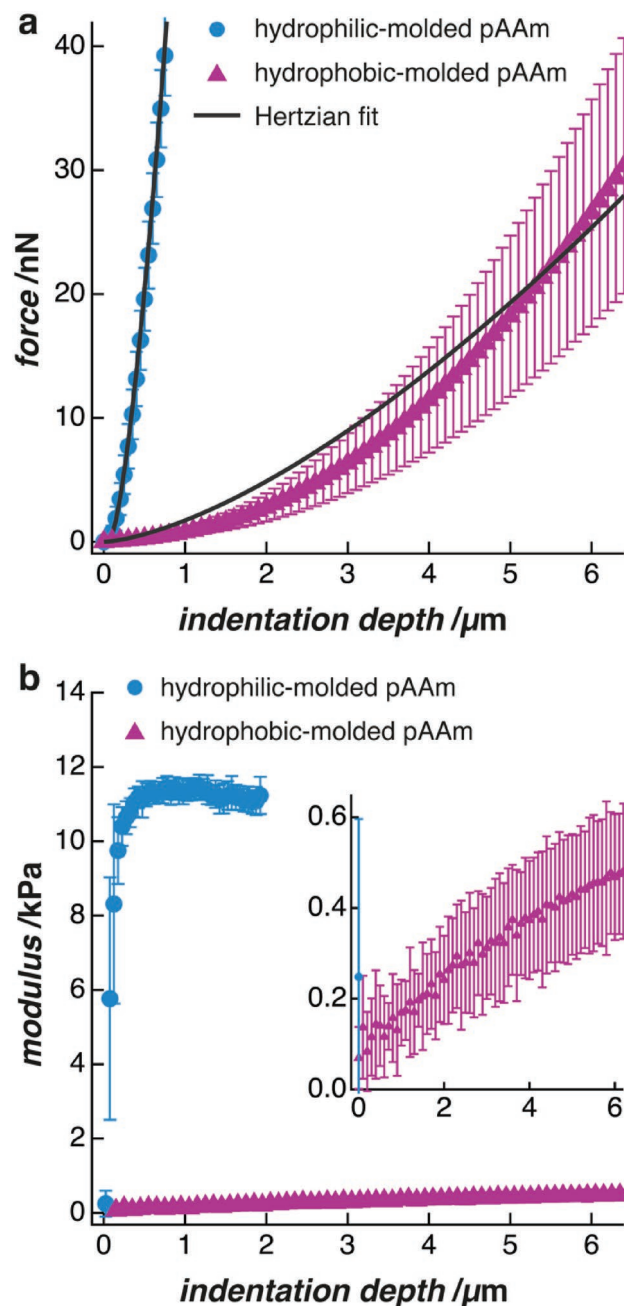


Figure 3. The AFM force–indentation curves a) with Hertzian fitting highlight the stiffness of the hydrophilic glass-molded (\bullet) pAAm surface in comparison to the markedly more compliant hydrophobic PDMS-molded (\blacktriangle) pAAm surface. In consequence, the modulus b) plateaus directly after indentation for the glass-molded (\bullet) pAAm hydrogel but increases gradually for the PDMS-molded (\blacktriangle) pAAm hydrogel.

2.3.2. Microindentation

In order to follow the dramatic difference in modulus progression of the contrasting hydrogel surfaces as we probe deeper into the bulk hydrogel; indentation experiments were continued using a microindenter. Here, the samples were indented to a depth of 100 μm .

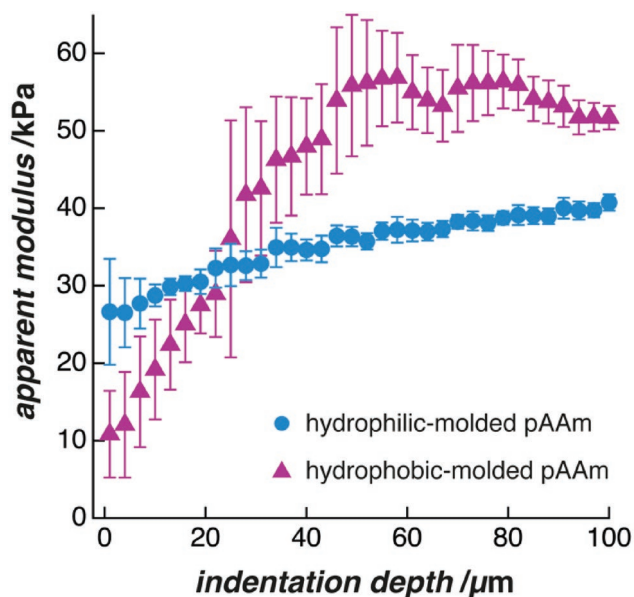


Figure 4. Force-indentation curves obtained with microindentation demonstrate significant differences in hydrogel polymer compressibility. The gradient in surface stiffness is significantly more pronounced for the hydrophobic PDMS-molded (\blacktriangle) than for the hydrophilic glass-molded (\bullet) pAAm hydrogel.

Classical Hertzian fitting of the indentation curves yielded a Young's modulus of 28.5 ± 0.8 kPa for the hydrophilic glass-molded hydrogel and of 27.2 ± 0.9 kPa for the hydrophobic PDMS-molded hydrogel. The minor difference between these two values was due to the slight mismatch between the Hertzian fit and the raw data on the softer, hydrophobic-molded hydrogel. Overall, these values show that both hydrogel samples have the same bulk mechanical properties. Thus, we conclude that the bulk of the pAAm hydrogels is unaffected by the molding condition.

In contrast, the Hertzian fits of single segments of the indentation curves, which we used to address the modulus evolution with indentation depth, drew contrasting pictures of the two hydrogel surfaces. Here, we showed that the apparent modulus (combination of poroelastic, viscoelastic, and elastic components that change continuously with surface depth) of the hydrophilic-molded hydrogel rose steadily for only 14 kPa over the indented 100 μm distance (Figure 4). This low and continuous rise in modulus indicates that the hydrogel polymer network is distributed evenly throughout the sample. The increase in apparent modulus of only 14 kPa over this extended indentation range shows an increasing stiffness with penetration distance. The overshoot of the apparent modulus over the Young's modulus of the bulk hydrogel indicates that we have compressed the entire hydrogel surface range into the bulk hydrogel. The apparent modulus of the hydrophobic-molded hydrogel rose steeply from a soft 11 kPa at contact point by a factor of 5 of the initial value at an indentation depth of 55 μm . This indicates that the outer layer is very compressible. Thus, we observed an extensive compressibility range for the hydrophobic-molded hydrogel surface. From this, we conclude that the amount of hydrogel polymer increases and its cross-linking density evolves with surface depth.

In conclusion, we find a comparably stiff hydrogel surface with a small gradient in apparent modulus and continuous, low compressibility after hydrophilic glass molding. After hydrophobic PDMS molding, the hydrogel surface was substantially softer with an extended modulus range. These findings are in line with the strong modulus differences that we observe with AFM nanoindentation and our resulting interpretations regarding the decrease in mesh size with increase in total polymer volume fraction and cross-linking for the hydrophobic-molded gradient structure. Despite their contrasting mechanical properties at the surface, both samples have the same Young's modulus in the bulk with a remarkable degree of consistency.

2.4. Friction of pAAm Hydrogel in Gemini Contact

The friction of both hydrogel surfaces was measured, in order to investigate the influence of structural differences on the tribological behavior of the hydrogels. In order to do this in a real gemini contact, pin and disk were fabricated from hydrogels with identical molding histories. This ensured that virtually identical polymeric surface structures were in sliding contact. Figure 5 displays the evolution of friction coefficient with sliding velocity for both sample sets. The hydrophilic-molded hydrogel revealed speed-dependent frictional behavior. Here, the friction coefficient rose from 0.02 to 0.5 over two orders of magnitude in sliding velocity. The hydrophobic-molded hydrogel, on the other hand, showed an overall lower friction coefficient of 0.01. In this case, the friction coefficient remained constant over the entire velocity range tested in this work.

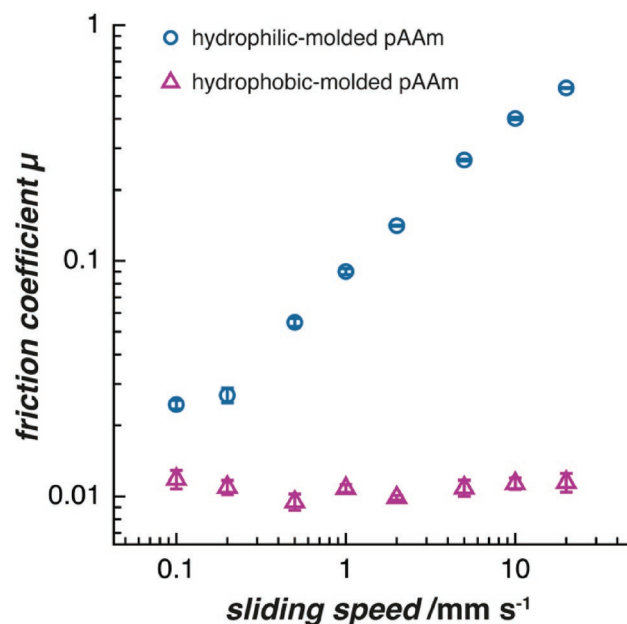


Figure 5. The two pAAm hydrogel surfaces show contrasting tribological behavior in gemini contact: the friction coefficient of the hydrophilic glass-molded pAAm hydrogel (\circ) increases with speed, whereas the friction coefficient of hydrophobic PDMS-molded pAAm hydrogel (\triangle) remains constant over the entire speed range of 0.1–20 mm s^{-1} .

Here, we show that hydrogels with the same chemistry and equal Young's modulus of the bulk exhibit entirely different tribological characters. The speed-dependent, higher friction of the hydrophilic glass-molded hydrogel contrasts with the speed-independent, low friction of the hydrophobic PDMS-molded hydrogel. The only disparity between the samples, which could have led to such marked differences in tribological behavior, lies in their surface structures as described above.

3. Conclusion

In this work, we experimentally demonstrate a very pronounced gradient of continuously increasing polymer volume fraction and correspondingly decreasing water content as we move from the surface of hydrophobic-molded hydrogels into the bulk. This extended gradient, which stretches over a range of 50 μm from the surface into the bulk hydrogel, is characterized by a very soft top surface and an increasing apparent modulus and polymer volume fraction as a function of sample depth. At the interface, this hydrogel is covered with a water-rich film (Figure 6). The combination of low polymer volume fraction and the substantial water film at the immediate surface renders the hydrophobic-molded hydrogel highly lubricious, independent of sliding speed.

While the apparent modulus of the bulk hydrogel proves to be independent of the molding history, the surface of hydrophilic-molded hydrogels differs significantly from those with a hydrophobically induced gradient structure. Hydrogels with a hydrophilic molding history reveal only a shallow gradient at their surface. The polymer volume fraction on such surfaces is only slightly diminished compared to the bulk and increases rapidly over a small distance to form the bulk hydrogel. A liquid film, as it forms at the interface of hydrophobic-molded hydrogels, is not found for this sample type (Figure 6). Consistent with the bulk-like, high polymer volume fraction at the surface, this hydrogel is characterized by its low compressibility and an increasing friction coefficient with sliding speed.

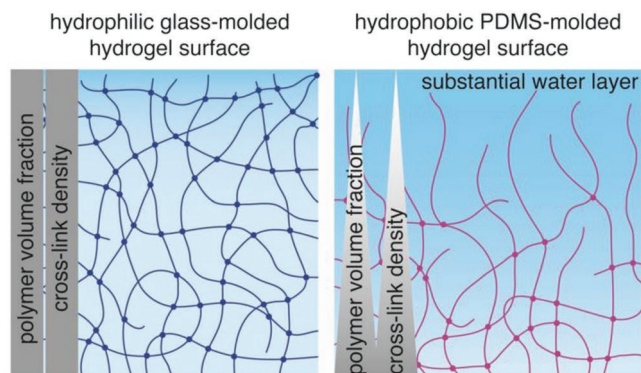


Figure 6. Hydrophilic glass-molded pAAm hydrogels (left) are characterized by a polymer surface structure similar to that of the bulk hydrogel. In contrast, pAAm hydrogels molded against a hydrophobic PDMS counter-surface show a distinct gradient of increasing polymer volume fraction and cross-linking with a decrease of water from the surface towards the bulk hydrogel. At the immediate surface, these hydrogels possess a substantial water layer that governs their surface properties.

Our work provides experimental evidence that the polymer volume fraction at the hydrogel surface, independent of its polymer volume fraction in the bulk, is the decisive factor for the tribological properties of this class of materials. As the water content at a hydrogel surface is directly related to its polymer volume fraction, our demonstration of the substantial water film at the interface of hydrophobic-molded hydrogels is in accordance with other studies that predict more lubricious hydrogel surfaces with higher water contents. Furthermore, the ability to hold water at the surface even under static conditions raises the question as to whether it is sufficient to relate hydrogel lubrication to the classical picture of soft elasto-hydrodynamic lubrication, in order to capture the behavior of this complex system. Based on our results, it seems more reasonable to assume a combination of different mechanisms for hydrogel tribology, as is recognized to be the case for cartilage.^[2,11]

Even though it is beyond the scope of this work to fully reveal the relationship between polymer volume fraction and mesh size, exact knowledge of the mesh size evolution with sample depth is a key point for guiding the tribological response of hydrogels in the future. By providing a detailed picture of the polymer network density, the combination of polymer volume fraction and cross-linking density, at hydrogel surfaces, this work provides insights that can lead to a more complete understanding of the relationship between mesh size and hydrogel friction in the future.

4. Experimental Section

Mold Preparation: To create distinct surfaces from chemically identical bulk hydrogels, hydrogels were polymerized against molds with contrasting surface energies. For hydrophilic hydrogel molding, glass microscope slides (Menzel-Gläser, Thermo Scientific, US) were used, which were cleaned with piranha solution prior to hydrogel polymerization, to ensure that water contact angles were below 5°. For hydrophobic hydrogel molding, sheets of PDMS (1:10 curing agent to base, SYLGARD 184 silicone elastomer, base, and curing agent, Dow Corning, USA) were used with water contact angles above 100°. After curing at 65 °C for 24 h, all uncross-linked polymer chains were extracted by immersion of the PDMS sheets in toluene for 1 week. The toluene was exchanged every day and replaced by ethanol (EtOH) stepwise.^[12] The extracted PDMS was vacuum-dried and stored in a desiccator. Prior to use, it was rinsed with EtOH and blown dry in a stream of nitrogen.

Hydrogel Polymerization: pAAm hydrogels were synthesized by the free radical polymerization of 7.5 wt% of the monomer acrylamide (AAm, Sigma-Aldrich, $\geq 99\%$), 0.3 wt% of the cross-linker *N,N'*-methylenebis(acrylamide) (MBAm, Sigma-Aldrich, $\geq 99.5\%$), 0.01 wt% of the catalyst tetramethylethylenediamide (TEMED, Sigma-Aldrich, 99%), and 0.01 wt% of the initiator ammonium persulfate (APS, Sigma-Aldrich, $\geq 98\%$) in a deoxygenated environment (concentration of $\text{O}_2 < 100$ ppm). All stock solutions and final hydrogels were prepared with deuterium oxide (D_2O , Sigma-Aldrich, 99 atom% D). The use of D_2O , instead of H_2O , improved the contrast between liquid phase and polymer phase in neutron reflectometry measurements later on. After gentle mixing of the stock solutions to final concentrations, the polymerizing solution was poured into the glass and PDMS molds to form 2 mm thick samples. After 24 h, the polymerized hydrogels were demolded and immersed into an excess amount of D_2O to allow for equilibrium swelling.

Mold Characterization: The surface roughness of PDMS and glass molds was determined by means of AFM (Naio AFM, Nanosurf, Switzerland). Mold sample areas of $10 \times 10 \mu\text{m}$ were scanned before and after use in hydrogel polymerization. Three areas were scanned per sample and three samples were investigated per mold.

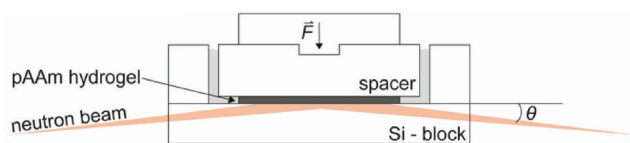


Figure 7. Cross section of the experimental setup for neutron-reflectometry measurements, depicting the hydrogel, pressed onto a silicon block with force F while fully immersed in D_2O . The neutron beam illuminates the sample at an angle θ with a beam footprint slightly smaller than the sample size.

The surface wettability of the molds was determined by water dynamic contact angle (DCA) measurements (DSA 100, Krüss GmbH, Germany) in an automated procedure. For advancing (θ_a) contact angles, the water-drop volume was increased from 4 to 10 μL in two steps. Videos of 175 frames were recorded for each step. For receding (θ_r) contact angles, the drop volume was decreased from 10 to 0 μL in one step with video recording of 500 frames. The speed of all measurements was 15 $\mu\text{L min}^{-1}$. Three different locations were measured on each mold. For evaluation, video sequences of moving drops were fitted with a tangent method 2 fit routine, with a fourth-order polynomial function (Drop-Shape Analysis program, DSA3 software, Krüss).

Neutron Reflectometry: Neutron-reflectometry measurements were carried out at the Swiss Spallation Neutron Source (SINQ) at the Paul-Scherrer Institute (Villigen, Switzerland). The apparatus for multiportional reflectometry (AMOR) was used in time-of-flight detection mode. Neutron reflectivity data at the hydrogel surface were recorded at a neutron wavelength range of $3.5 \text{ \AA} < \lambda < 12 \text{ \AA}$ at incident angles of $\theta = -0.5^\circ$ and $\theta = -1.4^\circ$ and a beam footprint of $50 \times 16 \text{ mm}^2$. Samples slightly larger than the beam footprint were placed on a polished and piranha-cleaned silicon block of $100 \times 50 \times 10 \text{ mm}^3$ and surrounded by a poly(tetrafluoroethylene) (PTFE) liquid cell (Figure 7). The hydrogels were immersed in D_2O to prevent sample drying during the measurements. The samples were compressed onto the Si crystal with weights, corresponding to forces of 0, 5, and 11 N, and measurements were recorded in random order. Each measurement, carried out at room temperature, lasted 3 h, in order to reach a satisfactory neutron signal-to-noise ratio.

The sample reflectivity was calculated as the ratio of the reflected and incident beam intensities. The reflectivity profiles were fitted and analyzed using a theoretical model based on the Parratt formalism.^[13] This took multiple reflections from a layered sample into account and allowed the researchers to determine the layer thicknesses and polymer volume fractions with sample depth. A vertical distribution of SLD was assumed and fitted to match the experimental data. The SLD of pure D_2O is $6.36 \times 10^{-6} \text{ \AA}^{-2}$. The SLD of pure pAAm was significantly smaller than that of pure D_2O . This was taken into account by considering the SLDs of both the monomer and cross-linker and their ratio in the polymer network, as well as the water-to-polymer ratio of the swollen hydrogel. In this way, the SLD of the sample system could be limited to a minimum value of $6 \times 10^{-6} \text{ \AA}^{-2}$ for accuracy of these fits. A measurement resolution of $\Delta q_z/q_z = 0.05$, with q_z being the momentum transfer vector, was determined for all fits.

Infrared Spectroscopy: ATR-FTIR spectra were collected on a Bruker Optics Alpha system (Bruker, USA) with a built-in diamond ATR spectrometer. Hydrogel samples were placed in a PTFE sample holder around the ATR crystal and immersed in D_2O to ensure equilibrium hydration during a measurement. The experimental setup was the same as for neutron-reflectometry measurements (Figure 1). The samples were compressed onto the crystal with weights, corresponding to forces of 0, 5, 13, and 18 N. Taking into account the deformation of the hydrogel under load, these forces correspond to pressures of 0.8, 4.8, 9.7, and 12.0 kPa. The weights were exchanged between single measurements in random order. For each sample and weight combination, three spectra were acquired (64 scans, resolution 4 cm^{-1} , wavenumber range $4000\text{--}500 \text{ cm}^{-1}$). The background of the spectra was pure D_2O . Analysis of the data was carried out with OPUS 6 software from Bruker.

Nanoindentation: Nanoindentation experiments were performed on an AFM (MFP3D, Asylum Research, Santa Barbara, USA). To determine the normal spring constant, k , of the Au-coated tipless cantilever (NSC-36, Micromash, Estonia), Sader's method was used.^[14] A silica microsphere (GP0083, Whitehouse Scientific, Waverton, UK) with radius $12.5 \mu\text{m}$ was glued to the end of the tipless cantilever for indentation experiments. The spring constant k of the cantilever was then corrected for the colloid position and determined to be $k' = 2.24 \text{ N m}^{-1}$.^[15] Prior to measurements, the optical lever sensitivity was calibrated by pressing the probe against the hard surface of a clean silicon wafer fully immersed in the measurement liquid. All indentation experiments were carried out in liquid to eliminate the influence of capillary forces on the measurement results. We chose 4-(2-hydroxyethyl)-1-piperazineethanesulfonic acid (HEPES) buffer solution with a pH of 7.43 and an ionic strength of $10 \times 10^{-3} \text{ M}$ as measurement liquid to minimize the influence of electrostatic forces from the silica microsphere.

Force-indentation curves were acquired on hydrophilic glass- and hydrophobic PDMS-molded hydrogel samples, fully immersed in HEPES I. Several force maps of 2×3 force curves over an area of $60 \times 60 \mu\text{m}^2$ were recorded with indentation speeds of $1 \mu\text{m s}^{-1}$ on several locations of each sample.

The elastic modulus of a sample was derived by fitting the Hertzian model to each force-indentation curve^[16]

$$F = \frac{4E \times R^{0.5}}{3(1-\nu^2)} \times d^{1.5} \quad (1)$$

Here F is the measured force, E is the elastic modulus of the sample, R is the indenter radius, ν is the Poisson's ratio and d is the indentation depth. The Poisson's ratio was set to 0.5, assuming incompressibility for hydrogels at the instant of indentation.^[17] The contact point d_0 of pin and sample surface in a force-indentation curve was identified as the position of the z-piezo stage at which the force upon approach deviated from zero by more than the average force noise of 0.1 nN. This strategy for exact contact-point determination could be applied because there were no adhesive or repulsive forces upon approach. The indentation depth at any point of indentation was calculated as the position of the z-piezo minus the cantilever deflection at that depth. To obtain the evolution of the elastic modulus as a function of indentation depth, d in the Hertzian model was replaced by $d-d_0$ and the force-indentation curves were divided into small sections that were fitted separately.

Microindentation: Microindentations were carried out on a custom-built indentation and friction measurement device described in detail by Dunn et al.^[18] The pin, a borosilicate glass sphere of 1 mm radius, was attached to a double leaf-flexure spring with a spring constant of $k = 165.9 \mu\text{N } \mu\text{m}^{-1}$. Hydrophilic glass-molded and hydrophobic PDMS-molded pAAm hydrogels were indented to a depth of 100 μm in four consecutive steps of 25 μm with a 10 min waiting time between steps. This indentation strategy was applied to record the strong relaxation effect of the samples, observed especially on the hydrophobic-molded hydrogel. The indentation speed was $4 \mu\text{m s}^{-1}$ and a sequence of 15 indents was carried out at each spot. Three indentation spots were distributed over a sample area of $1.5 \times 1.5 \text{ cm}^2$. All experiments were carried out in HEPES I buffer at room temperature.

The derivation of the Young's modulus from microindentations followed the same procedure as the analysis of the nanoindentations. The following adaptations to the above-described procedure had to be made: first, the average force noise was corrected to the instrument-specific value of 0.5 μN for the identification of the contact point d_0 . Second, the hydrogel relaxation between indentation steps was measured, and subtracted from the immediate elastic response of the hydrogel upon indentation. A detailed description of this procedure and the derivation of the apparent modulus can be found in the Supporting Information. All force-indentation curves except for the first one were analyzed at every indentation spot. This procedure was applied to avoid a possible overestimation of E from hydrogel damage caused by stress concentration at the first indentation.^[19]

Friction in Gemini Contact: Friction tests in gemini contact were performed in a reciprocating configuration (CSEM Tribometer, Neuchâtel,

Switzerland). The pin—a hydrogel disk with a diameter of 10 mm—was slid over a countersubstrate of the same sample type (glass-molded vs glass-molded pAAm and PDMS-molded vs PDMS-molded pAAm) in flat-on-flat contact. Pin and substrate had a thickness of about 3 mm each, and the setup was fully immersed in ultrapure water. The selected normal load on the pin was 0.5 N, which corresponds to ≈ 6 kPa of contact pressure. This pressure range matches the pressure range of an eyelid in contact with the cornea or a contact lens.^[20] Sliding speeds were varied sinusoidally for each test from 0.1 to 20 mm s⁻¹ at a fixed sliding amplitude of 5 mm. All measurements were recorded at room temperature.

Only the last six to ten cycles of each test were evaluated, in order to account for the running-in of the samples. For the determination of the friction coefficient, μ , no more than 20% of the middle position of each friction cycle was analyzed, corresponding to a constant velocity of $\pm 2\%$ within the sinusoidal velocity profile of a complete cycle.

Supporting Information

Supporting Information is available from the Wiley Online Library or from the author.

Acknowledgements

The authors thank Prof. G Sawyer, Prof. A. Pitenis and Dr. J.M. Uruña for generously sharing their expertise in hydrogels and tribometers. This work was financed by the European Research Council (ERC) under the European Union's Horizon 2020 research and innovation program (Grant Agreement No. 669562).

Conflict of Interest

The authors declare no conflict of interest.

Keywords

hydrogels, lubrication, polymer volume fraction, substrate effects, surface structures

Received: July 31, 2019

Revised: September 4, 2019

Published online: October 14, 2019

- [1] a) W. Hunter, *Philos. Trans. R. Soc.*, A **1742**, 42, 514; b) E. S. Jones, *Lancet* **1936**, 227, 1043; c) P. R. Lewis, C. W. McCutchen, *Nature* **1959**, 184, 1285; d) C. W. McCutchen, *Wear* **1962**, 5, 1.
- [2] a) R. Crockett, *Tribol. Lett.* **2009**, 35, 77; b) G. A. Ateshian, *J. Biomech.* **2009**, 42, 1163; c) S. Jahn, J. Seror, J. Klein, *Annu. Rev. Biomed. Eng.* **2016**, 18, 235; d) D. L. Burris, A. C. Moore, *Biotribology* **2017**, 12, 8; e) D. L. Burris, L. Ramsey, B. T. Graham, C. Price, A. C. Moore, *Tribol. Lett.* **2019**, 67, 46.
- [3] O. Wichterle, D. Lim, *Nature* **1960**, 185, 117.
- [4] A. S. Hoffman, *Adv. Drug Delivery Rev.* **2012**, 64, 18.
- [5] a) E. Porte, P. Cann, M. Masen, *J. Mech. Behav. Biomed.* **2019**, 90, 284; b) J. Kim, A. C. Dunn, *Soft Matter* **2016**, 12, 6536.
- [6] a) J. Gong, Y. Osada, *J. Chem. Phys.* **1998**, 109, 8062; b) J. P. Gong, Y. Osada, *Prog. Polym. Sci.* **2002**, 27, 3.
- [7] J. P. Gong, *Soft Matter* **2006**, 2, 544.
- [8] A. A. Pitenis, W. G. Sawyer, *Tribol. Lett.* **2018**, 66, 113.
- [9] a) J. P. Gong, A. Kii, J. Xu, Y. Hattori, Y. Osada, *J. Phys. Chem. B* **2001**, 105, 4572; b) M. Peng, J. Ping Gong, Y. Osada, *Chem. Rec.* **2003**, 3, 40.
- [10] M. Peng, T. Kurokawa, J. P. Gong, Y. Osada, Q. Zheng, *J. Phys. Chem. B* **2002**, 106, 3073.
- [11] a) M. A. Accardi, D. Dini, P. M. Cann, *Tribol. Int.* **2011**, 44, 565; b) B. N. J. Persson, M. Scaraggi, *Tribol. Lett.* **2017**, 66, 23; c) B. T. Graham, A. C. Moore, D. L. Burris, C. Price, *J. Biomech.* **2018**, 71, 271.
- [12] A. Hourlier-Fargette, A. Antkowiak, A. Chateauminois, S. Neukirch, *Soft Matter* **2017**, 13, 3484.
- [13] L. G. Parratt, *Phys. Rev.* **1954**, 95, 359.
- [14] J. E. Sader, J. W. M. Chon, P. Mulvaney, *Rev. Sci. Instrum.* **1999**, 70, 3967.
- [15] R. J. Cannara, M. Eglin, R. W. Carpick, *Rev. Sci. Instrum.* **2006**, 77, 053701.
- [16] a) D. C. Lin, F. Horkay, *Soft Matter* **2008**, 4, 669; b) H. Hertz, *J. Reine Angew. Math.* **1881**, 92, 156.
- [17] R. H. Pritchard, P. Lava, D. Debruyne, E. M. Terentjev, *Soft Matter* **2013**, 9, 6037.
- [18] a) A. C. Dunn, J. M. Uruña, Y. C. Huo, S. S. Perry, T. E. Angelini, W. G. Sawyer, *Tribol. Lett.* **2013**, 49, 371; b) A. Dunn, W. G. Sawyer, T. Angelini, *Tribol. Lett.* **2014**, 54, 59.
- [19] a) R. E. Webber, C. Creton, H. R. Brown, J. P. Gong, *Macromolecules* **2007**, 40, 2919; b) T. L. Sun, T. Kurokawa, S. Kuroda, A. B. Ihsan, T. Akasaki, K. Sato, M. A. Haque, T. Nakajima, J. P. Gong, *Nat. Mater.* **2013**, 12, 932.
- [20] A. J. Shaw, B. A. Davis, M. J. Collins, L. G. Carney, *IEEE T. Bio-Med. Eng.* **2009**, 56, 2512.